

Efficient Mode Transfer on a Compact Silicon Chip by Encircling Moving Exceptional Points

Qingjie Liu,¹ Shuyi Li¹, Bing Wang^{1,*}, Shaolin Ke,² Chengzhi Qin,¹ Kai Wang,¹ Weiwei Liu,¹
Dingshan Gao^{1,†}, Pierre Berini^{4,5,‡} and Peixiang Lu^{1,2,3,§}

¹*School of Physics and Wuhan National Laboratory for Optoelectronics, Huazhong University of Science and Technology, Wuhan 430074, China*

²*Hubei Key Laboratory of Optical Information and Pattern Recognition, Wuhan Institute of Technology, Wuhan 430205, China*

³*CAS Center for Excellence in Ultra-Intense Laser Science, Shanghai 201800, China*

⁴*School of Electrical Engineering and Computer Science, University of Ottawa, Ottawa, Ontario K1N 6N5, Canada*

⁵*Department of Physics and Center for Research in Photonics, University of Ottawa, Ottawa, Ontario K1N 6N5, Canada*



(Received 19 October 2019; accepted 18 March 2020; published 16 April 2020)

Exceptional points (EPs) are branch point singularities of self-intersecting Riemann sheets, and they can be observed in a non-Hermitian system with complex eigenvalues. It has been revealed recently that dynamically encircling EPs by adiabatically changing the parameters of a system composed of lossy optical waveguides could lead to asymmetric (input-output) mode transfer. However, the length of the waveguides had to be considerable to ensure adiabatic evolution. Here we demonstrate that the parameters can change adiabatically along a smaller encircling loop by utilizing moving EPs, leading to significant shortening of the structures compared to fixed EPs. Meanwhile, the mode transmittance is remarkably improved and the transfer efficiency persists at $\sim 90\%$. Moving EPs are very promising for applications such as highly integrated broadband optical switches and convertors operating at telecommunication wavelengths.

DOI: [10.1103/PhysRevLett.124.153903](https://doi.org/10.1103/PhysRevLett.124.153903)

The Hamiltonian of a nonconservative system containing open boundaries or dissipation is non-Hermitian [1–4]. By tuning two (or more) parameters of the system, the eigenvalues can be made to move on a Riemann surface, of which branch point singularities are known as exceptional points (EPs) [4–7]. There have been a diversity of intriguing effects based on EPs such as loss induced transparency [8], lasing [9–11], and unidirectional reflection [12]. The topological features of EPs have also been studied theoretically and experimentally in exciton-polariton systems [13], coupled acoustic cavities [14], and microwave cavities [15,16]. When adiabatically changing the parameters of a system around an EP in parametric space, the initial eigenstate will transfer to another while gaining a geometric phase [17–20]. In photonics, the dynamical evolution of eigenstates can be realized by slowly changing the geometry and (effective) permittivity of a dielectric waveguide and has found applications in asymmetric (input-output) mode transfer [21–26], where the nature of the output mode is only determined by the encircling direction rather than the nature of the input mode. Experimental demonstrations have been implemented in optomechanical systems [21], microwave waveguides [25], and ferromagnetic waveguides [26]. Very recently, mode transfer by dynamically encircling EPs has been demonstrated in coupled dielectric waveguides at optical telecommunication wavelengths [27]. However, the length of the waveguides was considerable given the

need to satisfy the adiabaticity condition, which limits the potential for use in highly integrated optical devices.

In order to reduce the waveguide length, the encircling loop should be narrowed while ensuring that the parametric evolution remains adiabatic [28–30]. However, if the EP remains fixed in parameter space, narrowing the loop may not be possible as the EP might become excluded from the loop. Here we propose, design, and fabricate a non-Hermitian optical waveguide system based on subwavelength gratings (SWGs) [31–33] to demonstrate a moving EP in the system. An advantage of waveguides based on SWGs is that the optical parameters of every SWG segment (effective index, propagation loss) can be precisely controlled. As the parameters encircle in parametric space, the EP can move and remain enclosed transiently by the encircling loop. In this way, we are able to reduce the length of the waveguide by several factors. Our study provides a new method for researches on the topological property of non-Hermitian systems.

Considering an optical waveguide doublet composed of two closely spaced waveguides, the amplitudes of the modes in the individual waveguides satisfy the coupled-mode equation

$$-i \frac{d}{dz} \begin{pmatrix} A_1 \\ A_2 \end{pmatrix} = H \begin{pmatrix} A_1 \\ A_2 \end{pmatrix} = \begin{pmatrix} \alpha_1 & C \\ C & \alpha_2 + i\gamma \end{pmatrix} \begin{pmatrix} A_1 \\ A_2 \end{pmatrix}, \quad (1)$$

where H is the Hamiltonian of the system, $A_{1,2}$ stand for the mode amplitudes in the individual waveguides, $\alpha_{1,2}$ are the

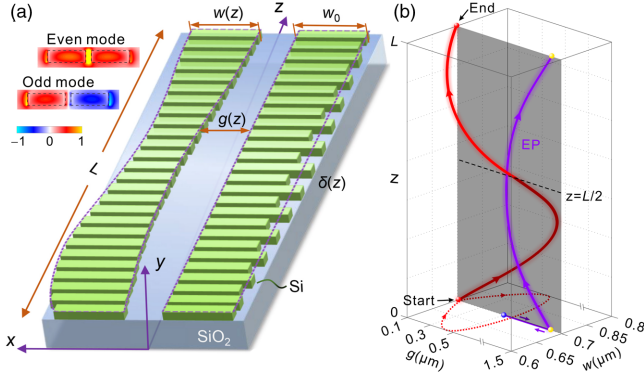


FIG. 1. (a) Schematic of the SWG waveguide doublet. (Insets) Profiles of the even and odd modes at both ends of the structure. (b) Three-dimensional plots of the encircling curve (red) and trajectory of EPs (purple) along the waveguide doublet. The projection of the encircling curve constitutes a round loop (red dotted) in the (g, w) plane.

propagation constants, γ is the propagation loss, and C is the coupling coefficient. Generally, the eigenvalues of the Hamiltonian are complex-valued but they coalesce as $\Delta\alpha = \alpha_1 - \alpha_2 = 0$ and $C = \gamma/2$, at the EP. In practice, the waveguides are constituted by SWGs operating in the transverse-electric-like (TE) modes [34,35]. The SWG waveguide doublet is fabricated by patterning a Si layer with a thickness of 220 nm on the buried SiO₂ substrate [36–39], as shown in Fig. 1(a). Only the fundamental TE mode is allowed in each SWG waveguide. The lateral profiles of the even and odd modes at both ends of the waveguides are also shown, which are formed by symmetric and antisymmetric coupling of the fundamental modes in individual SWG waveguides. The modes can be excited by using an asymmetric directional coupler with incidence from different ports [36,37]. The details of mode excitation are provided in the Supplemental Material [40]. The period and filling factor of the SWGs are fixed to $\Lambda = 0.3 \mu\text{m}$ and $f = 0.565$, respectively. The operating photon energy, corresponding to the telecommunication wavelength around $\lambda = 1550 \text{ nm}$, is far below the band gap of the SWGs such that Bragg scattering is avoided [35,39]. One SWG waveguide has a slowly varying width $w(z)$ along z and the other has an average width w_0 but is periodically corrugated by a small amplitude δ , which introduces loss due to scattering and is parametrized as $\gamma(\delta)$. The relation between γ and δ is discussed in the Supplemental Material [40]. The width and gap of the waveguides vary as $w(z) = w_0 \pm \Delta w \sin(2\pi z/L)$ and $g(z) = g_0 + \Delta g \sin(\pi z/L)$, where $w_0 = 0.7$, $\Delta w = 0.1$, and $g_0 = 0.1 \mu\text{m}$. As the propagation distance increases from $z = 0$ to L , the parametric variation gives rise to a circular loop in the (g, w) plane with its size tuned by Δg .

For a small but fixed loss, the EP is far from the starting point of the loop such that the loop must be large enough to encircle the EP. Thus, the waveguide should be rather

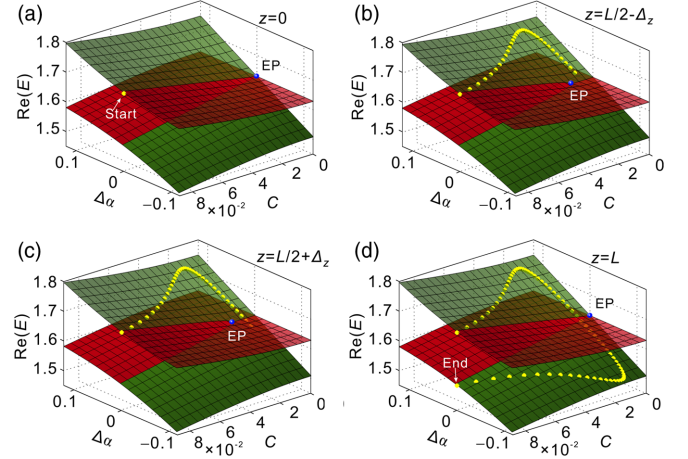


FIG. 2. (a)–(d) Evolution of the Riemann sheets and the EP as a function of parameter variation in the $(C, \Delta\alpha)$ plane. $\Delta_z = 0.01L$. The yellow and blue dots show the clockwise trajectory of instantaneous eigenvalue and EP, respectively. The mode at the start (end) point is the even (odd) mode.

lengthy to guarantee adiabatic evolution. On the other hand, for larger loss, the EP can be encircled by a smaller parameter loop, but the modes suffer considerable attenuation during propagation. In this regard, the loss of the waveguide is set to be variable following the corrugation distribution $\delta(z) = \delta_0 \exp[-(z - L/2)^2 G_0^2 / L^2]$ with $\delta_0 = 0.1 \mu\text{m}$ and $G_0 = 3.5$. Figure 1(b) shows the three-dimensional plots of parametric and EP variations along the waveguide. The branch of the Riemann surface in (g, w) parameter space indicates an initial EP at $g = 1.4$ and $w = 0.7 \mu\text{m}$ as $z = 0$, which is out of the parameter encircling loop. As the propagation distance increases, the EP moves along a curved trajectory in the $w = 0.7 \mu\text{m}$ plane since the location of the EP is independent of w , given the EP condition $C(g) = \gamma(\delta)/2$. It becomes closest to the parametric loop as $z = L/2$ and $\delta = \delta_0$, where $g_{\text{EP}} = 0.52$ and $w_{\text{EP}} = 0.7 \mu\text{m}$. To have this transient EP encircled by the parameter loop in the (g, w) plane, we should ensure $\Delta g > g_{\text{EP}}(\delta_0) - g_0 = 0.42 \mu\text{m}$.

To shed light on the process of mode transfer, the eigenvalue and EP evolution on the Riemann surface are illustrated in Fig. 2. For convenient observation, we map the eigenvalues from the (g, w) plane to the $(C, \Delta\alpha)$ plane considering that C and $\Delta\alpha$ are functions of g and w , respectively. The encircling loop starts from the initial point at $z = 0$, where $C = C(g_0)$ and $\Delta\alpha = 0$, as shown in Fig. 2(a). With increasing propagation distance, the eigenvalue moves on the upper Riemann sheet. As the encircling point reaches the crossing of the two Riemann sheets, the EP has moved within the loop (encircled), and the eigenvalue progresses smoothly to the lower sheet, as shown in Figs. 2(b) and 2(c). After a round trip, the EP moves out of the loop, as shown in Fig. 2(d). Generally, instantaneous mode transfer occurs only when the Riemann sheets are just glued together such that the encircling point

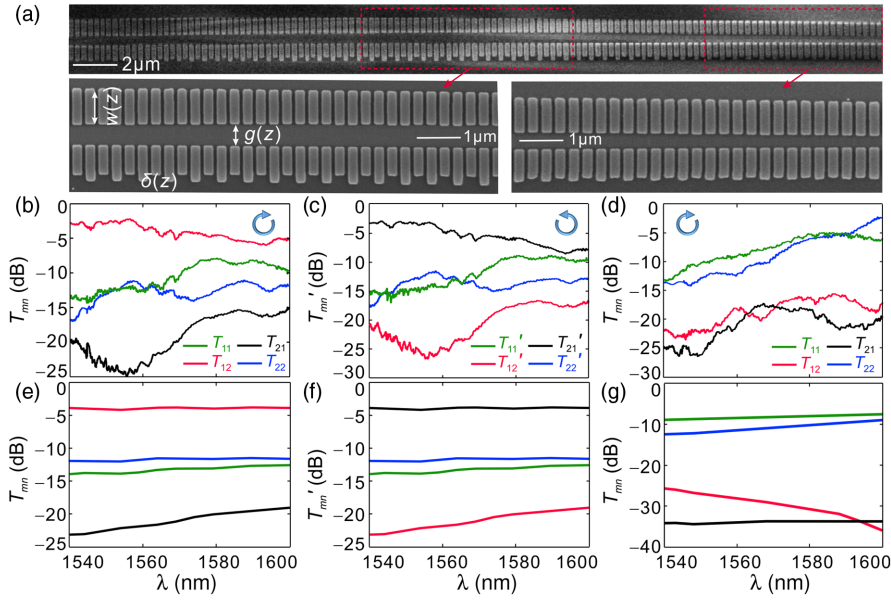


FIG. 3. (a) SEM images of the central part of the fabricated SWG waveguide doublet. (b)–(d) Experimentally measured and (e)–(g) FDTD-simulated spectral response of transmittances T_{mn} (T'_{mn}) for clockwise (anticlockwise) encircling. The modulation amplitude of the gap is set to (b), (c), (e), (f) $\Delta g = 0.45 \mu\text{m}$ and to (d), (g) $\Delta g = 0.1 \mu\text{m}$.

can temporally pass through the crossing of distinct sheets. Even if the EP is not included in the encircling loop at its starting and end points, topological mode transformation persists.

The structure [Fig. 1(a)] was fabricated using electron-beam lithography and reactive ion etching. The experimental setup and measurement techniques are discussed in the Supplemental Material [40]. Figure 3(a) gives scanning electron microscope images of the fabricated structure. The length of the waveguide doublet is $L = 69 \mu\text{m}$ and the gap variation amplitude is $\Delta g = 0.45 \mu\text{m}$. Figures 3(b) and 3(c) plot the measured spectral mode transmittance for different encircling directions. T_{mn} (T'_{mn}) signifies the transmittance from input mode m to output mode n as the mode is injected from left (right), where $m, n = 1$ or 2 , denoting the even or odd mode, respectively. The oscillations in the spectra are due to reflection from connections of the SWG waveguides and convertors [44,45]. As the even mode is incident from the left, we have $T_{12} \gg T_{11}$ and the difference can be as large as 9 dB in the range 1540–1565 nm, which means that the odd mode dominates at the output and most of the even mode transfers to the odd. As the odd mode is incident, we have $T_{22} \gg T_{21}$, and the odd mode still dominates at the output. Consequently, for left incidence, corresponding to clockwise encircling [Fig. 3(b)], the odd mode dominates at the output for either the odd or even injection. On the other hand, as the mode is injected from the right, corresponding to anticlockwise encircling [Fig. 3(c)], the even mode dominates at the output—one observes that $T'_{11} \gg T'_{12}$ and $T'_{21} \gg T'_{22}$ for injection of the even and odd modes, respectively. Interestingly, the transmittance with mode transfer is always larger than that

without mode transfer; that is, $T_{12} \gg T_{22}$ and $T'_{21} \gg T'_{11}$. This is due to reciprocity [46,47], which indicates $T'_{mn} = T_{nm}$. For clockwise encircling as shown in Fig. 3(b), the odd mode always dominates at the output ($T_{12} \gg T_{11}$). Thus, we have $T_{21} \gg T_{11}$. On the other hand, there is $T'_{21} \gg T'_{22}$ as depicted in Fig. 3(c), which leads to $T_{12} \gg T_{22}$ for clockwise encircling.

We have also performed control experiments for $\Delta g = 0.1 \mu\text{m}$, where the encircling loop does not enclose the EP. As shown in Fig. 3(d), one sees that $T_{11} \gg T_{12}$ and $T_{22} \gg T_{21}$, which means that no mode transfer occurs. This result repeats for anticlockwise encircling. The measured transmittance spectra coincide well with those obtained by finite-difference time-domain (FDTD) simulations over the wavelength range of 1540–1565 nm, as given in Figs. 3(e)–3(g). The transmittances are remarkably improved by about 10 dB compared to a design based on a fixed EP [40]. Over the wavelength range of 1565–1600 nm, the experimental and simulated results are inconsistent, mainly because the ancillary optical circuits in the experiments do not operate well at wavelengths far away from the design wavelength of 1550 nm. Nevertheless, from Figs. 3(b) and 3(c), it is observed that the output mode is only determined by the encircling direction over a wide operating wavelength range of 60 nm in the telecommunications band (near 1550 nm).

The electric field distributions in the waveguide doublet obtained by FDTD simulations are given in Fig. 4. The fields are normalized in each propagation direction to evidently reveal the mode transfer process. When the even and odd modes are injected from the left, we always obtain the odd mode at the output, as observed from the

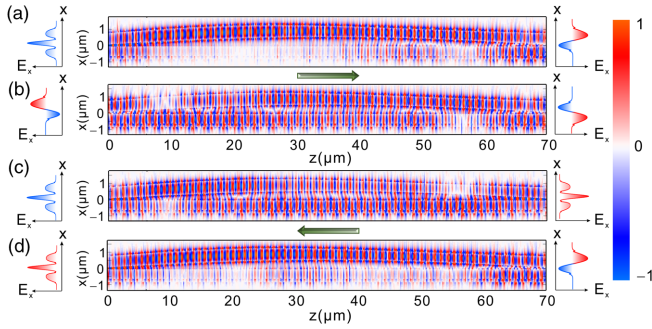


FIG. 4. (a)–(d) Numerically simulated E_x field distributions in the SWG waveguide doublet. The incident mode is injected from (a),(b) the left side and (c),(d) the right side. The insets at the ends of the structure show the computed field profile along the x direction at the input and output ports.

distribution of the output electric field (E_x), which is out of phase on the two SWG waveguides, as shown in Figs. 4(a) and 4(b). Alternatively, when the even and odd modes are injected from the right, the even mode with an in-phase field distribution is observed at the left output, as shown in Figs. 4(c) and (d).

The asymmetric mode transfer results from the non-adiabatic evolution induced by loss [17–20]. We denote the local eigenmode at position z by $\varphi_n(z)$ and the eigenvalue by $\beta_n(z)$ as the even ($n = 1$) or odd ($n = 2$) mode is incident. Because of the nonadiabatic transitions, the total field should be the superposition of the two local modes: $\psi(z) = \sum_n a_n(z)\varphi_n(z)$, where a_n represents the mode amplitude. Figures 5(a) and 5(b) plot the intensity weighted mode index $\beta(z) = \sum_n \text{Re}[\beta_n(z)]|a_n(z)|^2 / \sum_n |a_n(z)|^2$ for distinct encircling directions, which illustrates mode evolution in practice. For encircling clockwise [Fig. 5(a)], we always have $\beta(L) = \beta_1(L)$ at the output ($z = L$) for incidence of either even or odd modes. For even mode incidence, the evolution of β follows $\beta_1(z)$ almost completely, indicating that the mode conversion abides by an adiabatic evolution. On the other hand, for odd mode incidence, β varies with β_2 initially, then switches abruptly to β_1 at the middle of the waveguide. This nonadiabatic transition is due to the distinct losses of modes φ_1 and φ_2 during propagation. As β_1 has a much smaller imaginary part than β_2 , the evolution of $\beta_1(z)$ undergoes smaller power damping and always dominates in the mode transfer. For anticlockwise encircling [Fig. 5(b)], the process is reversed, with the output always being the even mode. Similarly, the evolution of $\beta_2(z)$ undergoes smaller power damping and dominates in the mode transfer. The mismatch of the dynamic and adiabatic evolutions is due to incomplete mode transfer, which can be improved by using a longer waveguide [40].

The efficiency of mode transfer can be characterized by the power ratio of output modes [21]. Figure 5(c) plots the power ratio of the odd mode $\eta_{12} = T_{12}/(T_{12} + T_{11})$ as a function of the waveguide length L for clockwise encircling

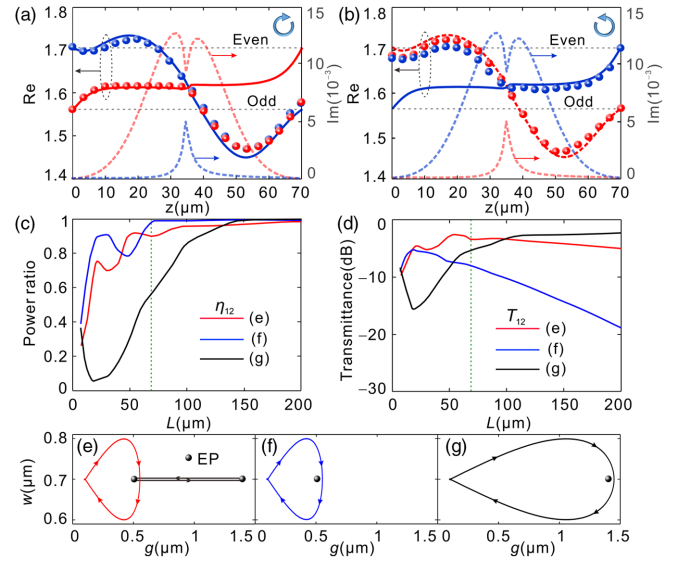


FIG. 5. (a),(b) Evolution of the instantaneous eigenvalues $\beta_{1,2}(z)$ and intensity weighted eigenvalue $\beta(z)$ during parameter encircling of EP. The solid (real) and dashed (imaginary) curves denote adiabatic evolutions of $\beta_{1,2}(z)$ (blue for β_1 and red for β_2) and the dots denote dynamical evolution of $\beta(z)$. (c) Power ratio η_{12} and (d) transmittance T_{12} as functions of the waveguide length for encircling moving and fixed EPs. The vertical dashed line indicates the waveguide length $L = 69 \mu\text{m}$ in the experiment. (e) Parameter encircling as the EP moves from $g_{\text{EP}} = 1.40$ to $0.52 \mu\text{m}$ and back again. Encircling fixed EPs at (f) $g_{\text{EP}} = 0.52$ and (g) $g_{\text{EP}} = 1.40 \mu\text{m}$. All EPs located at $w_{\text{EP}} = 0.70 \mu\text{m}$.

and even mode incidence. The other cases are shown in the Supplemental Material [40]. Here we aim to compare the transfer efficiency by encircling moving and fixed EPs, as depicted in Figs. 5(e)–5(g). The corresponding transmittance T_{12} is also shown in Fig. 5(d). The results are obtained by FDTD simulations at $\lambda = 1550 \text{ nm}$. For fixed EPs, the loss is distributed evenly in the waveguide. As the EP locates closely to the starting point of encircling loop, the transfer efficiency reaches unity rapidly as L increases, but the transmittance is relatively low. For a distant EP, the mode evolution suffers less loss, but the loop size should be large enough to enclose the EP. Thus, the nonadiabatic evolution dominates for shorter waveguide and the transfer efficiency is much lower. The efficiency is further reduced for odd mode incidence [40]. Comparably, encircling a moving EP results in both high transfer efficiency $\sim 90\%$ and considerable transmittance (-3.4 dB) as $L = 69 \mu\text{m}$. The values coincide well with the experimental results in Fig. 3(b).

In conclusion, we have experimentally realized dynamic encircling of an EP in SWG waveguides. The EP moves in parameter space as the third parameter is introduced and modulated along the length. Even if the EP at its initial position is not enclosed by the encircling loop, mode transfer still persists as long as the EP moves within the encircling loop during passage of the encircling point

(eigenvalue) and that the latter can pass through the crossing of the two Riemann sheets. Allowing the EP to move via loss modulation enables the transferred mode to take over $\sim 90\%$ of the total output power, while significantly reducing the loss and length of the structure. Encircling a moving EP provides a new scheme to optimize performance, diminish length, and diminish insertion loss, while maintaining the topological properties of the operation.

The work is supported by the National Natural Science Foundation of China (Grants No. 11674117, No. 11974124, and No. 11374115) and the National Postdoctoral Program for Innovative Talent (Grant No. BX20190129).

Q. L. and S. L. contributed equally to this work.

* wangbing@hust.edu.cn

† dscao@hust.edu.cn

‡ berini@eecs.uottawa.ca

§ lupeixiang@hust.edu.cn

- [1] C. M. Bender and S. Boettcher, *Phys. Rev. Lett.* **80**, 5243 (1998).
- [2] M. V. Berry, *Czech. J. Phys.* **54**, 1039 (2004).
- [3] I. Rotter, *J. Phys. A* **42**, 153001 (2009).
- [4] B. Zhen, C. W. Hsu, Y. Igarashi, L. Lu, I. Kaminer, A. Pick, S. Chua, J. D. Joannopoulos, and M. Soljačić, *Nature (London)* **525**, 354 (2015).
- [5] B. Dietz, H. L. Harney, O. N. Kirillov, M. Miski-Oglu, A. Richter, and F. Schäfer, *Phys. Rev. Lett.* **106**, 150403 (2011).
- [6] M. V. Berry, *J. Opt.* **13**, 115701 (2011).
- [7] M. V. Berry and R. Uzdin, *J. Phys. A* **44**, 435303 (2011).
- [8] A. Guo, G. J. Salamo, D. Duchesne, R. Morandotti, M. Volatier-Ravat, V. Aimez, G. A. Siviloglou, and D. N. Christodoulides, *Phys. Rev. Lett.* **103**, 093902 (2009).
- [9] L. Feng, Z. J. Wong, R.-M. Ma, Y. Wang, and X. Zhang, *Science* **346**, 972 (2014).
- [10] B. Peng, Ş. K. Özdemir, M. Liertzer, W. Chen, J. Kramer, H. Yilmaz, J. Wiersig, S. Rotter, and L. Yang, *Proc. Natl. Acad. Sci. U.S.A.* **113**, 6845 (2016).
- [11] B. Peng, Ş. K. Özdemir, S. Rotter, H. Yilmaz, M. Liertzer, F. Monifi, C. M. Bender, F. Nori, and L. Yang, *Science* **346**, 328 (2014).
- [12] Q. Liu, B. Wang, S. Ke, H. Long, K. Wang, and P. Lu, *Opt. Express* **25**, 7203 (2017).
- [13] T. Gao *et al.*, *Nature (London)* **526**, 554 (2015).
- [14] K. Ding, G. Ma, M. Xiao, Z. Q. Zhang, and C. T. Chan, *Phys. Rev. X* **6**, 021007 (2016).
- [15] C. Dembowski, H. D. Gräf, H. L. Harney, A. Heine, W. D. Heiss, H. Rehfeld, and A. Richter, *Phys. Rev. Lett.* **86**, 787 (2001).
- [16] C. Dembowski, B. Dietz, H.-D. Gräf, H. L. Harney, A. Heine, W. D. Heiss, and A. Richter, *Phys. Rev. E* **69**, 056216 (2004).
- [17] R. Uzdin, A. Mailybaev, and N. Moiseyev, *J. Phys. A* **44**, 435302 (2011).
- [18] T. J. Milburn, J. Doppler, C. A. Holmes, S. Portolan, S. Rotter, and P. Rabl, *Phys. Rev. A* **92**, 052124 (2015).
- [19] H. Menke, M. Klett, H. Cartarius, J. Main, and G. Wunner, *Phys. Rev. A* **93**, 013401 (2016).
- [20] S. Ke, B. Wang, C. Qin, H. Long, K. Wang, and P. Lu, *J. Lightwave Technol.* **34**, 5258 (2016).
- [21] H. Xu, D. Mason, L. Jiang, and J. G. E. Harris, *Nature (London)* **537**, 80 (2016).
- [22] A. U. Hassan, B. Zhen, M. Soljačić, M. Khajavikhan, and D. N. Christodoulides, *Phys. Rev. Lett.* **118**, 093002 (2017).
- [23] Y. Choi, C. Hahn, J. W. Yoon, S. H. Song, and P. Berini, *Nat. Commun.* **8**, 14154 (2017).
- [24] S. N. Ghosh and Y. D. Chong, *Sci. Rep.* **6**, 19837 (2016).
- [25] J. Doppler, A. A. Mailybaev, P. Rabl, N. Moiseyev, and S. Rotter, *Nature (London)* **537**, 76 (2016).
- [26] X. L. Zhang, S. Wang, B. Hou, and C. T. Chan, *Phys. Rev. X* **8**, 021066 (2018).
- [27] J. W. Yoon *et al.*, *Nature (London)* **562**, 86 (2018).
- [28] H. Wang, L. J. Lang, and Y. D. Chong, *Phys. Rev. A* **98**, 012119 (2018).
- [29] A. Laha, A. Biswas, and S. Ghosh, *Phys. Rev. Applied* **10**, 054008 (2018).
- [30] M. Kang, J. Chen, and Y. D. Chong, *Phys. Rev. A* **94**, 033834 (2016).
- [31] P. Cheben, P. J. Bock, J. H. Schmid, J. Lapointe, S. Janz, D.-X. Xu, A. Densmore, A. Delage, B. Lamontagne, and T. J. Hall, *Opt. Lett.* **35**, 2526 (2010).
- [32] P. Cheben, D.-X. Xu, S. Janz, and A. Densmore, *Opt. Express* **14**, 4695 (2006).
- [33] J. Čtyroký, J. G. Wangüemert-Pérez, P. Kwiecien, I. Richter, J. Litvik, J. H. Schmid, Í. Molina-Fernández, A. Ortega-Moñux, M. Dado, and P. Cheben, *Opt. Express* **26**, 179 (2018).
- [34] P. Cheben, R. Halir, J. H. Schmid, H. A. Atwater, and D. R. Smith, *Nature (London)* **560**, 565 (2018).
- [35] H. Yun, Y. Wang, F. Zhang, Z. Lu, S. Lin, L. Chrostowski, and N. A. F. Jaeger, *Opt. Lett.* **41**, 3041 (2016).
- [36] D. Dai, J. Wang, and Y. Shi, *Opt. Lett.* **38**, 1422 (2013).
- [37] C. Li, D. Liu, and D. Dai, *Nanophotonics* **8**, 227 (2019).
- [38] S. Li, Y. Zhou, J. Dong, X. Zhang, E. Cassan, J. Hou, C. Yang, S. Chen, D. Gao, and H. Chen, *Optica* **5**, 1549 (2018).
- [39] H. Yun, L. Chrostowski, and N. A. F. Jaeger, *Opt. Lett.* **43**, 1935 (2018).
- [40] See Supplemental Material at <http://link.aps.org/supplemental/10.1103/PhysRevLett.124.153903> for more details on the derivation of loss and coupling coefficients, the experimental setup and measurement, and additional simulation results of different encircling loops, which includes Refs. [41–43].
- [41] C. Fietz, Y. Urzhumov, and G. Shvets, *Opt. Express* **19**, 19027 (2011); G. Parisi, P. Zilio, and F. Romanato, *Opt. Express* **20**, 16690 (2012).
- [42] L.-W. Luo, N. Ophir, C. P. Chen, L. H. Gabrielli, C. B. Poitras, K. Bergmen, and M. Lipson, *Nat. Commun.* **5**, 3069 (2014); Y. Ding, J. Xu, F. D. Ros, B. Huang, H. Ou, and C. Peucheret, *Opt. Express* **21**, 10376 (2013); X. Chen, C. Li, C. K. Y. Fung, S. M. G. Lo, and H. K. Tsang, *IEEE Photonics Technol. Lett.* **22**, 1156 (2010); D. Dai and

- J. E. Bowers, *Nanophotonics* **3**, 283 (2014); D. Dai and H. Wu, *Opt. Lett.* **41**, 2346 (2016); C. Li and D. Dai, *J. Lightwave Technol.* **36**, 2129 (2018).
- [43] A. U. Hassan, G. L. Galmiche, G. Harari, P. LiKamWa, M. Khajavikhan, M. Segev, and D. N. Christodoulides, *Phys. Rev. A* **96**, 052129 (2017).
- [44] R. Halir *et al.*, *Laser Photonics Rev.* **9**, 25 (2015).
- [45] A. Ortega-Moñux *et al.*, *Laser Photonics Rev.* **7**, L12 (2013).
- [46] Y. D. Chong, L. Ge, and A. D. Stone, *Phys. Rev. Lett.* **106**, 093902 (2011).
- [47] R. J. Potton, *Rep. Prog. Phys.* **67**, 717 (2004).